Peer-reviewed version available at Materials 2018, 11, 1158; doi:10.3390/ma11071158

Evolution of elevated-temperature strength and creep resistance during multi-step heat treatments in Al-Mn-Mg alloy

G. S. Wang[1, 2], K. Liu[3]*, S. L. Wang[1, 2]

[1]Key Laboratory of Electronmagnetic Processing of Materials, Ministry of Education, Northeastern University, Shenyang, P. R. China, 110004

[2]School of Materials Science and Engineering, Northeastern University, Shenyang, P. R. China, 110004

[3]Department of Applied Science, University of Quebec at Chicoutimi, Saguenay, QC, Canada, G7H 2B1

* Corresponding author: kun.liu@uqac.ca; Tel.:1-4185455011 ext. 7112

Abstract:

Present work has systematically investigated the evolution of dispersoid and elevated-temperature properties including the strength and creep resistance during the various multi-step heat treatments in Al-Mn-Mg 3004 alloys. Results show that only α-Al(MnFe)Si dispersoid is observed in the studied temperature range (up to 625°C) and it coarsens with increasing temperature to 500°C but dissolves at 625°C. The evolution of elevated-temperature strength and creep resistance is greatly related to the temperature of each step during the multi-step heat treatments. Generally, lower temperature at the first-step heat treatment leads to higher properties while the properties decrease with increasing temperature of last-step heat treatment. Suitable models have been introduced to explain the evolution of strength and the creep threshold stress at elevated-temperature during the various heat treatments.

Keywords: Al-Mn-Mg alloy; Dispersoids; Heat treatment; Elevated temperature; Strength; Creep resistance.

1. Introduction

Nowadays, the applications of dispersoid-strengthen aluminum alloys are increasing in the automotive and aerospace industries due to the formation of thermal-stable dispersoids at elevated temperature (250-350°C) [1, 2]. It is reported that the coherent or semi coherent Al_3M dispersoids can precipitate and thermal stable up to 250-350°C through the addition of transition and rare earth elements, such as individual or combined addition of Sc, Zr and Er [3-6] . However, the high cost of these elements limits their wide application.

In the decades, the dispersoids have also been reported to precipitate in Al-Mn 3xxx alloy during the proper heat treatment and the precipitation behavior of dipsersoids has been fully investigated. It is reported that the yield strength of 3003 at room temperature (RT) after 375°C/24h has been improved to 80 MPa compared with 52MPa after

600°C/24h due to precipitation of dispersoids [7]. Recently, present authors have systematically studied the evolution of dispersoids at relative lower heat treatment temperature (300-425°C) and their influence on elevated-temperature properties in Al-Mn-Mg 3004 alloys [6, 8-12]. It is found that high volume fraction and well distributed α-Al(MnFe)Si dispersoids are observed after treated at 375℃ for 48h, leading to the remarkable improved YS and creep resistance at elevated-temperature. However, the applied heat treatment in above literature is limited to one-step at relative low temperature and limited open literature has been published about the evolution of dispersoids and elevated-temperature properties during the heat treatments at high temperature as well as multi-step heat treatments.

On the other hands, creep resistance is considered to be one of the most significant parameters in alloy application at elevated temperature [13-15]. Generally, the dislocation creep occurs in aluminum alloys at 250-350°C and the stress exponent and creep threshold stress has been well developed to explain the controlling mechanism during the creep test in aluminum alloys, especially in 1XXX alloys [16-19]. However, most of these literatures focus on the nano-scale precipitates or particles and the influence of bigger dispersoids (> 50 nm in diameter) on creep resistance has been less dealt with. Besides, little work has been performed on the creep resistance in Al-Mn 3xxx alloys and the evolution of creep threshold stress during the heat treatment is not fully discovered.

Therefore, in order to fully investigate the evolution of dispersoids during the various heat treatments and their influence on elevated-temperature strength and creep behaviors, the wide-temperature-range and multi-step heat treatments have been applied on Al-Mn-Mg 3004 alloy in present work and the strength and creep behaviors at 300°C have been measured and characterized. Meanwhile, suitable models are established to evaluate the relationship between dispersoids and elevated-temperature properties.

2. Experimental

2.1 Alloy preparation

Experimental 3004 alloy was prepared with commercially pure Al (99.7%) and pure Mg (99.9%), Al-25%Fe, Al-50%Si and Al-25%Mn master alloys. The chemical composition of the experimental 3004 alloy is Al-1.2%Mn-1.1%Mg-0.6%Fe-0.25%Si analyzed using optical emission spectrometer (OES).

In each test, approximately 3 kg of material was prepared in a clay-graphite crucible using an electric resistance furnace. The temperature of the melt was maintained at ~750°C for 30 min. The melt was degassed for 15 min and then poured into a permanent mold preheated at 250°C. The dimension of cast ingots was 30mm×40mm×80mm.

2.2 Heat treatment

According to our previous study [9], the onset precipitation temperature of dispersoids is around 340°C and the best condition can be obtained at 375°C/48h in the

range of 300-425°C. Therefore, another two higher temperature (500°C and 625°C) has been selected in present work and the condition of 375°C/48h is considered to be the base heat treatment in multi-step heat treatments. The heat treatments are performed in a programmable electric furnace with the temperature controller (± 2°C) and circulating air. The heating rate was set as 5°C/min. After each step, the ingots were directly quenched into water at RT. More detail of heat treatments are shown in Table 1.

Table 1 Parameters of heat treatments used in this study

Code	Parameter	Code	Parameter
A3	375°C/48h		
A5	500°C/10h	A6	625°C/4h
B53	500°C/10h+375°C/48h	B63	625°C/4h+375°C/48h
B35	375°C/48h+500°C/10h	B36	375°C/48h+625°C/4h
C353	375°C/48h+500°C/10h+375°C/48h	C363	375°C/48h+625°C/4h+375°C/48h

Note: "A" means single-step heat treatment while "B" and "C" stands for two-step and three-step heat treatment while the "3", "5"and "6" represent the heat treatment of "375°C/48h", "500°C/10h", and "625°C/4h".

2.3 Evolution of alloy properties

The precipitation behavior of dispersoids during precipitation treatment and thermal holding were evaluated by EC, Vickers microhardness and YS. EC was measured using a Sigmascope SMP10 electrical conductivity unit at RT, and the average value of 5 measurements was recorded for each sample. The mechanical property (YS) was obtained from compression tests performed on a Gleeble 3800 machine. Cylindrical specimens with a length/diameter ratio of 1.5 (i.e., 15 mm in length and 10 mm in diameter) were machined and tested at both RT and an elevated temperature (300°C) following the ASTM E9-89a standard. The total deformation of the specimens was set to 0.2, and the strain rate was fixed at 10^{-3} s^{-1}. For the compression test at 300°C, the specimen was heated to 300°C with a heating rate of 2°C/s and held for 3 minutes to stabilize. An average value of YS was obtained from 3 tests.

In addition, creep tests were performed at 300°C and specimens were the same size as the Gleeble samples. Creep behaviors were tested at a constant load of 38 MPa while another two loads (28 and 32 MPa) has been applied for the creep threshold stress and stress exponent. For each condition, 3 tests were repeated to confirm the reliability of the results.

2.4 Microstructure observation

The microstructural features including the intermetallics, dispersoids and grain structures for different conditions were observed by optical and electron microscopes. To reveal the dispersoids clearly, the polished samples were etched in 0.5% HF for 30 seconds. A scanning electron microscope (SEM, JSM-6480LV) equipped with an energy

dispersive x-ray spectrometer (EDS) and electron backscatter diffraction (EBSD) was used to examine the intermetallics and grain structure of the alloy under different conditions. A transmission electron microscope (TEM, JEM-2100) operated at 200kV was used to observe the distribution of dispersoids. The thickness of the TEM sample was measured with electron energy loss spectroscopy (EELS).The size and number density of dispersoids were measured using Clemex PE 4.0 image analysis software with the TEM images. In this study, the volume fraction of particle free zone (PFZ) was converted from the area fraction of PFZ measured in image analysis from optical images according to the Delesse's principle [20, 21] while the volume fraction of dispersoids was calculated according to the model introduced in the literature [22] and shown in Eq. (1):

$$V_v = A_A \frac{\overline{KD}}{\overline{KD} + t}(1 - A_{PFZ}) \quad (1)$$

where $\overline{D}$ is the average equivalent diameter of dispersoids; t is the TEM foil thickness; A_A is the area percentage of dispersoids from TEM observation; A_{PFZ} is the area percentage of the particle free zone (PFZ) from OM measurements; and $\overline{K}$ is the average shape factor of dispersoids.

3. Results and Discussion

3.1 Precipitation of dispersoids during the heat treatment

Though the $Al_6(MnFe)$ dispersoids have been reported to form when treated at 600°C in 3103 alloy [23], however, dispersoids after all the heat treatments performed in present work are identified as α-Al(MnFe)Si even at 600°C. As an example, Fig. 1 shows the dispersoids precipitated after A6 with the highest "H" temperature (625°C) and TEM-EDS result. As shown in Fig. 1a, the dispersoids can be present with different morphology, such as cubic and platelet-like. However, the TEM-EDS result (Fig. 1b) shows that all the dispersoids are composed of Mn, Fe and Si, identifying the dispersoids as α-Al(MnFe)Si. One of the likely reasons for free of $Al_6(MnFe)$ dispersoids in present work is the higher Si content in experimental 3004 alloy (0.25%) than the 3103 alloy in the literature (0.05%), which promotes the precipitation of α-Al(MnFe)Si dispersoids. Therefore, all the dispersoids talked about in the following part are referred to α-Al(MnFe)Si dispersoids.

Fig. 2 shows the distribution of dispersoids under single heat treatments (A3, A5 and A6). It displays that the finer α-Al(MnFe)Si dispersoids are uniformly precipitated after A3 (375°C/48h). Besides, only low volume fraction of PFZ can be observed surrounding the intermetallic particles (interdentritic zone) after A3, which can be attributed to the depletion of Mn near the intermetallics due to the formation of primary $Al_6(MnFe)$ and α-Al(MnFe)Si intermetallics. With increasing temperature to 500°C (Fig. 2b), the size of dispersoids becomes bigger. Meanwhile, PFZ begins to form in the center of dendrite arms, where some much bigger dispersoids present, indicating the coarsening of

dispersoids happens at 500°C compared with 375°C. However, little dispersoids can be observed with further increasing temperature to 625°C. As shown in Fig. 2c, only fragmented intermetallics are present in the Al matrix after A6 (625°C/4h). In the literature, it is reported that the α-Al(MnFe)Si dispersoids begin to dissolve at 600°C [22-24], hence it is reasonable for the dispersoids to dissolve into the matrix at 625°C.

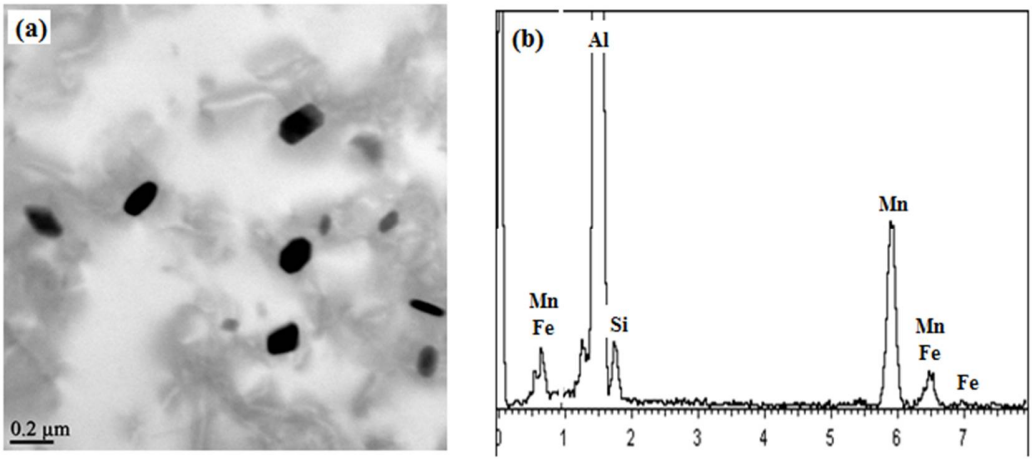

Fig. 1 Dispersoids after A6 and the TEM-EDS result

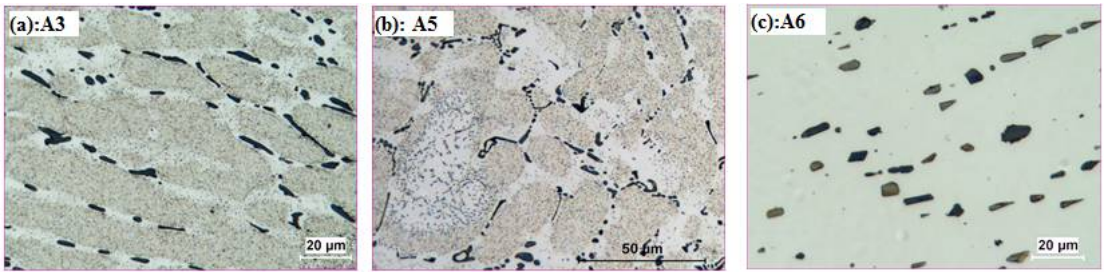

Fig. 2 Distribution of dispersoids after single-step heat treatment

The distribution of dispersoids after two-step and three-step heat treatments is shown in Fig. 3. Generally, coarsening of dispersoids happens when treated at 500°C, either under two or three steps heat treatment compared with A3. Besides, the volume fraction of PFZ increases after two or three steps heat treatment at 500°C. As shown in Table 2, the volume fraction of PFZ slightly increases from 32 vol. % in A5 to 37 vol. % in B35 but rapid to 45 vol. % in C353 and further to 55 vol. % in B53. The slightly increase in PFZ from A5 to B35 is mainly due to the dispersoids coarsening and more PFZ is shown in interdendrite zone (Fig. 3b). However, it can be found the volume fraction of bigger dispersoids in the center of dendrite arms increases after B53 (Fig. 3a) and C353 (Fig. 3c), leading to the higher volume fraction of PFZ.

However, the distribution of dispersoids after treated at 625°C is more complicit. As shown in Fig. 3d, the dispersoids are observed to distribute everywhere and PFZ is disappeared after B63, which is probably attributed to uniform soluted Mn atom in matrix after 625°C for 4h (homogenization). Similar phenomenon takes place after C363 (Fig. 3e), in which the dispersoids first precipitate in the first step at lower temperature

(375°C) and then dissolve into matrix in the second step at higher temperature (625°C) followed by the re-precipitate of uniformly-distributed dispersoids in the third step at lower temperature (375°C). However, it seems that the volume fraction of dispersoids after C363 is a little lower than B63, which is probably caused by decreasing soluted Mn concentration from incompletely dissolved dispersoids in second step, which is also shown in Fig. 3e. It is observed that there is still low volume fraction of dispersoids remaining after B36 (Fig. 3e) due to the incompletely dissolved dispersoids.

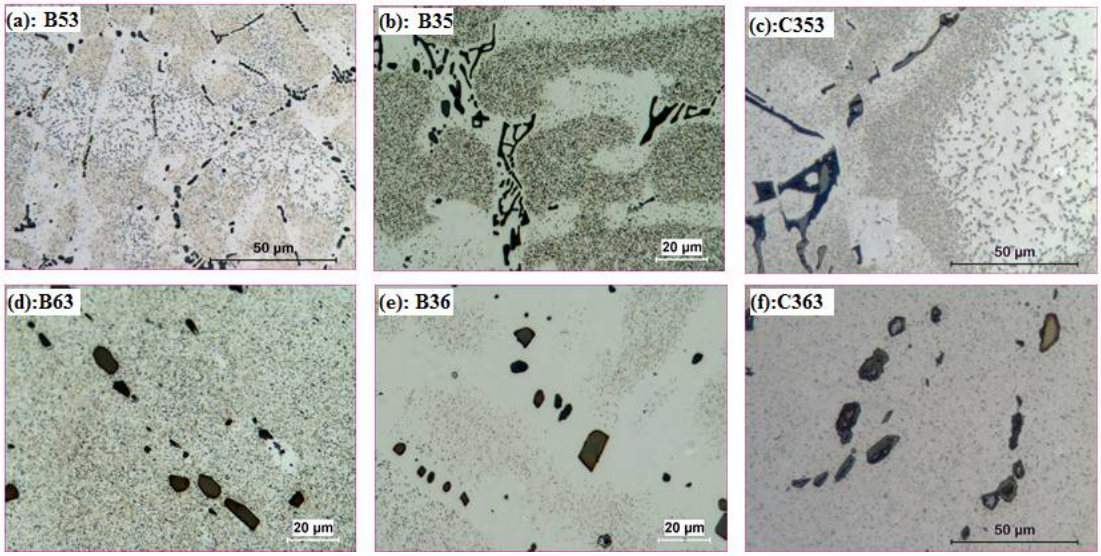

Fig. 3 Distribution of dispersoids after two-step and three-step heat treatment

In order to show more detail about the dispersoids, TEM has been performed and the distribution of dispersoids after various heat treatment is shown in Fig. 4. Similar to the distribution of dispersoids shown in Figs 2 and 3, the highest volume fraction of dispersoids precipitates in single treatment at lower temperature (A3 in Fig. 4a) and the coarsen dispersoids precipitate after treated at 500°C (A5 in Fig. 4b, B53 in Fig. 4d, and C353 in Fig. 4f). As shown in Table 2, the equivalent diameter of dispersoids after treated at 500°C is in the range of 107- 115 nm, which is much higher than in A3 (67 nm). Besides, the volume fraction of dispersoids varies with heat treatment and the highest is measured in B35, which is 1.67 vol. %, even higher than A5 (1.58 vol. %). This probably can be attributed to the first step heat treatment at lower temperature, in which the dispersoids has been fully precipitated and the relatively low coarsening rate of dispersoids at high temperature. However, some dispersoids are still observed after treated at 625°C for 4h (A6 in Fig. 4c) but the volume fraction is very low, which is just 0.27 vol. % (Table 2), which is different with the optical observation in Fig. 2c. Besides, the dipsersoids are also observed after B36 with a little higher volume fraction (0.51 vol. %) than A6, which agrees with the results obtained from Figs. 2 and 3. Furthermore, the interesting thing happens in condition B63 and C363, in which high volume fraction of dispersoids presents after etching in optical microscope observation (Figs. 3d and 3f)

but much lower volume fraction of dispersoids have been shown in TEM observation (Figs. 4g and 4i). The lower volume fraction after B63 and C363 under TEM is probably related to the phase transformation of intermetallics at high temperature. It is reported that $Al_6(MnFe)$ would transform to α-Al(MnFe)Si intermetallics at 600°C and the Mn/Fe ratio increases with holding time [25]. Therefore, partial Mn atoms diffuse to α-Al(MnFe)Si intermetallics during the phase transformation at high temperature, leading to the decreased soluted Mn concentration in matrix. Therefore, the drive force for the precipitation of dispersoids decreases with the decreasing supersaturation of Mn in matrix but Mn is uniformly distributed in the matrix. Therefore, dispersoids precipitate uniformly due to the homogenized Mn atom, in matrix but with lower volume fraction from lower Mn concentration in Al matrix in the last step at lower temperature (375°C) and it presents as the uniform distributed dispersoids in optical microscope without PFZ.

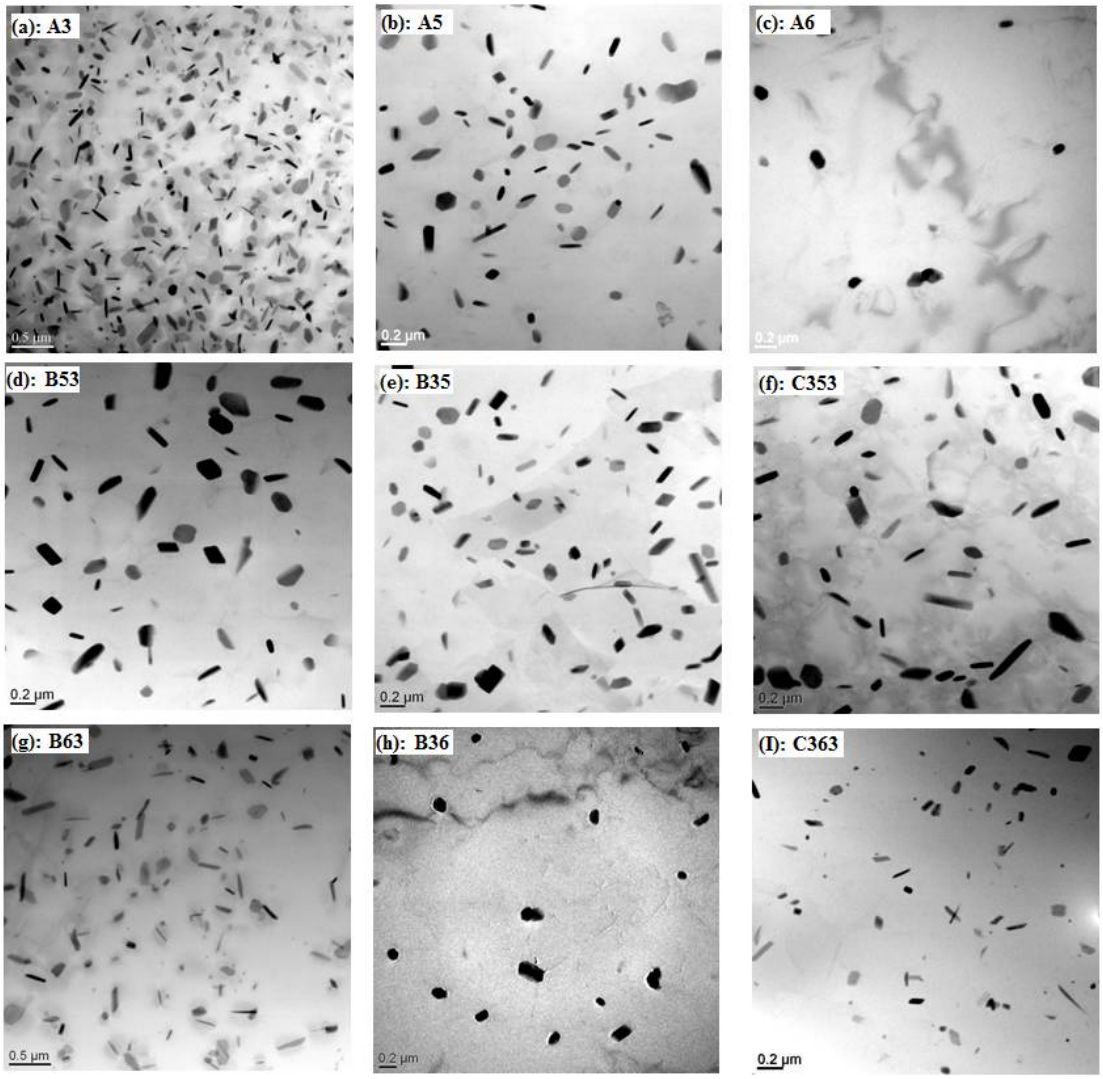

Fig. 4 Distribution of dispersoids during the heat treatment under TEM observation

Preprints (www.preprints.org) | NOT PEER-REVIEWED | Posted: 7 June 2018 doi:10.20944/preprints201806.0103.v1

Peer-reviewed version available at Materials 2018, 11, 1158; doi:10.3390/ma11071158

Table 2 Characters of dispersoids and PFZ during heat treatment

Code	Dispersoids		PFZ	Code	Dispersoids		PFZ
	Equivalent diameter nm	Volume fraction Vol.%	Volume fraction Vol. %		Equivalent diameter nm	Volume fraction Vol.%	Volume fraction Vol. %
A3	67(11)*	2.95(0.68)	28(3)				
A5	107(14)	1.58(0.52)	32(4)	A6	102(12)	0.27(0.13)	–
B53	112(15)	1.36(0.62)	55(8)	B63	82(15)	0.87 (0.15)	10(5)
B35	105(12)	1.67(0.54)	37(6)	B36	106(14)	0.51(0.21)	–
C353	111(21)	1.61(0.48)	45(7)	C363	83(12)	1.21(0.15)	8(6)

*Note: standard deviation is shown in bracket

3.2 Compression Yield Strength

As shown in Figs. 2-4, great changes happen on characters of dispersoids during the heat treatment, which will definitely affect the mechanical properties of alloys. Fig. 5 shows the typical true strain-stress curves of alloy after single step heat treatment (A3, A5 and A6) at both RT and 300°C.

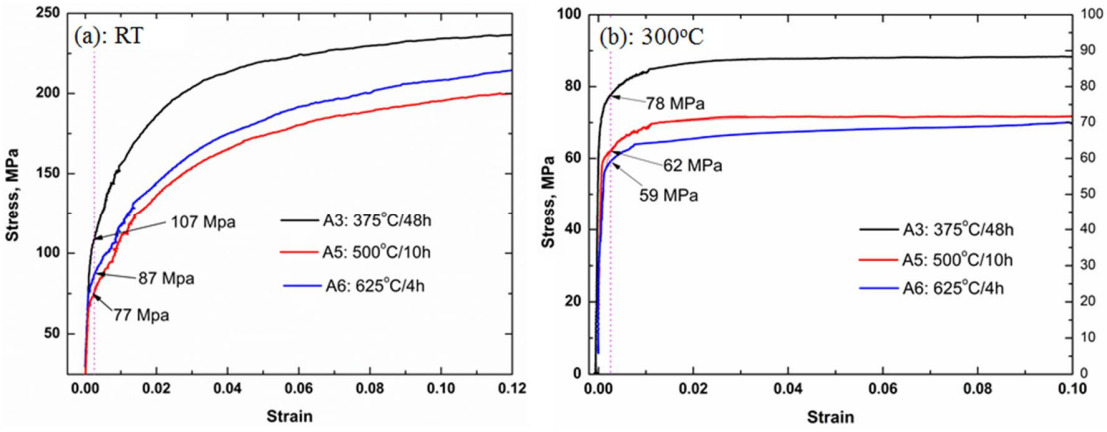

Fig. 5 True stain-stress curves of alloy after A3, A5 and A6 at both RT and 300°C

As shown in Fig. 5a, the compression YS at RT varies with A3, A5 and A6. The highest YS (108 MPa) is obtained in A3 due to the dispersoid strengthening from the highest volume fraction of dispersoids and YS decreases with the coarsening and decreasing volume fraction in A5 (77MPa). However, the YS of A6 is between A3 and A5 though with lowest volume fraction of dispersoids, which is attributed to the solid-solution strengthening from Mn in Al matrix. However, due to the weakened solution-hardening effect at 300°C (Fig. 5b), YS of A6 is lower than A5 and further lower than A3, which is 59 MPa in A6 to 62 MPa in A5 and 78 MPa in A3, as shown in Fig. 3b. The YS and EC of all the heat treatments are listed in Table 3.

Table 3 YS and EC after various heat treatments

Code	EC (% IACS)	YS (RT) (MPa)	YS (300°C) (MPa)	Code	EC (% IACS)	YS (RT) (MPa)	YS (300°C) (MPa)
A3	37.8 (0.3)*	107.9(3.5)	78.3(0.6)				
A5	39.2(0.5)	77.7 (2.3)	61.7(0.9)	A6	26.9 (0.8)	86.2(1.8)	59.3(1.6)
B53	38.1(0.6)	75.8(1.8)	58.2(0.5)	B63	38.3(0.5)	82.3(2.5)	60.9(1.4)
B35	38.9(0.5)	79.1(2.1)	63.9(1.1)	B36	27.9(0.5)	84.5(2.1)	61.9(1.9)
C353	37.9(0.2)	76.4(2.6)	58.6(0.5)	C363	38.1(0.6)	82.4(1.9)	62.3(1.5)

*Note: standard deviation is shown in bracket

As shown in Table 3, EC is mainly controlled by the last step, which is similar to the literature [24]. For instance, EC of A3, B53, B63, C353 and C363 is similar, which is around 38 %IACS. For the evolution of YS, it can be found that it decreases with increasing temperature, such as the descending YS in A3, A5 and A6. Besides, the first-step temperature plays a significant role in YS in multi-steps heat treatment, in which that YS is higher with lower first-step temperature than with higher first-step temperature. This can be proved from the YS between B35 and B53, B36 and B63 in Table 3.

In order to explain the evolution of YS at both RT and 300°C, two principal processes involved during the heat treatment have been considered in present work: precipitation of dispersoids at lower temperature (375°C and 500°C) for dispersoid strengthening and dissolution of dispersoids at high temperature (625°C) for solid-solution strengthening. Therefore, the evolution of YS can be estimated with the synergetic effect of these two factors.

According to the literature, the contribution of dispersoids to the YS of alloys (σ_D) can be estimated with Ashby-Orowan equation [7, 26]:

$$\sigma_D = \frac{0.84MGb}{2\pi(1-\nu)^{1/2}r}\ln\left(\frac{\gamma}{b}\right)\left(\frac{2\pi}{3f}\right)^{-1/2} \quad (1)$$

Where, M is the Taylor factor, G is the temperature-dependent matrix shear modulus (given as G=25.4[1-0.5(T-300)/933] [27]) while b, ν γ and f is the burgers vector of dislocation, poison ratio, radius and volume fraction of dispersoids , respectively.

On the other hand, the solid-solution strengthening from Mn atom is reported to have a liner relationship with soluted Mn concentration as [28]:

$$\sigma_{Mn} = HC^{\alpha} \quad (2)$$

Where, H and α is constant, which is 18.35 and 0.9 for soluted Mn atom under at RT while 10 and 0.8 at 300°C under the applied condition in present work (stain rate at 10^{-3} s^{-1} and total stain at 0.2%) [1, 28-30]. C is the concentration of soluted Mn atom is Al matrix and can be estimated using EC by neglecting the contribution of Fe and Si on EC due to their low solubility with the following equation [22]:

$$C = \left(\frac{1.74}{EC} - 0.0317\right)/0.033 \quad (3)$$

With above equations and characters of dispersoids in Table 2, the contribution of solid-soluted atom and dispersoids on YS can be estimated and the differences in YS (ΔYS) between A3 and other heat treatments have been calculated in present work and the comparison between calculated data and the experimental data is shown in Fig. 6. It can be seen that the tendency of evolution of YS at both RT and 300°C is the same between experimental and calculation data. However, the match between experimental and calculation is closer at RT (Fig. 6a) than at 300°C (Fig. 6b), which can be attributed to the more active on the movement of dislocation at 300°C. Besides, a bigger difference between calculated and experimental data is observed in the conditions of A6 and B36, in which the Mn is fully soluted in matrix at higher temperature (625°C) at both RT and 300°C, which are the last two points in Fig. 6. The reason is unclear but it is likely due to the formation of "solute drag" from Mn and Mg atoms [31-33], which hinders the movement of dislocation and then lead to the further increase of strength.

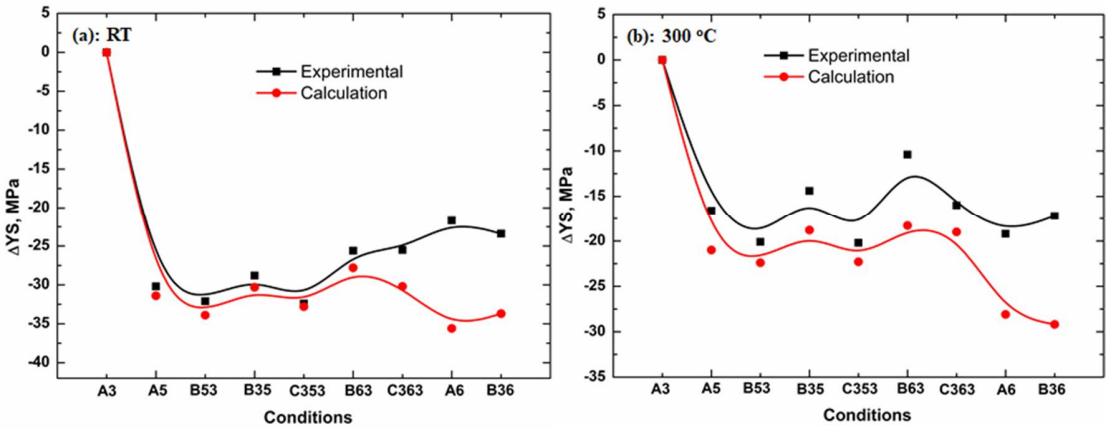

Fig. 6 Difference of YS between A3 and other heat treatments at RT and 300°C

3.3 Creep resistance

In our previous study [9], it is found that dispersoids have great effect on creep resistance. The creep tests at 300°C after heat treatments also have been performed in present work and the results are shown in Fig. 7. It displays that the total creep strain is greatly related to the heat treatment. Generally, the total strain treated at 625°C is much less than 500°C, such as the B53 in Fig. 7a and B63 in Fig. 7b. It can be found the creep stain has reached to the limitation of creep machine (indicted by the red arrow in Fig. 7a, also in C353) after 55 hours in B53 but it is only 0.152 in B63 after 100 hours, showing the different role of soluted atoms and dispersoids on the creep property. Besides, the creep stain seems lower after heat treatment involved the first step with lower temperature (375°C), such as B35 and B53 in Fig. 7a, B36 and B63 in Fig. 7b, which is similar to the evolution of YS shown in Table 3 and Fig. 6. Furthermore, though the highest YS at 300°C is obtained in A6 (Table 3), the minimum creep stain is obtained in

A3, which has the finest but the highest volume fraction of dispersoids, further confirming the significant positive influence of dispersoids on the creep resistance.

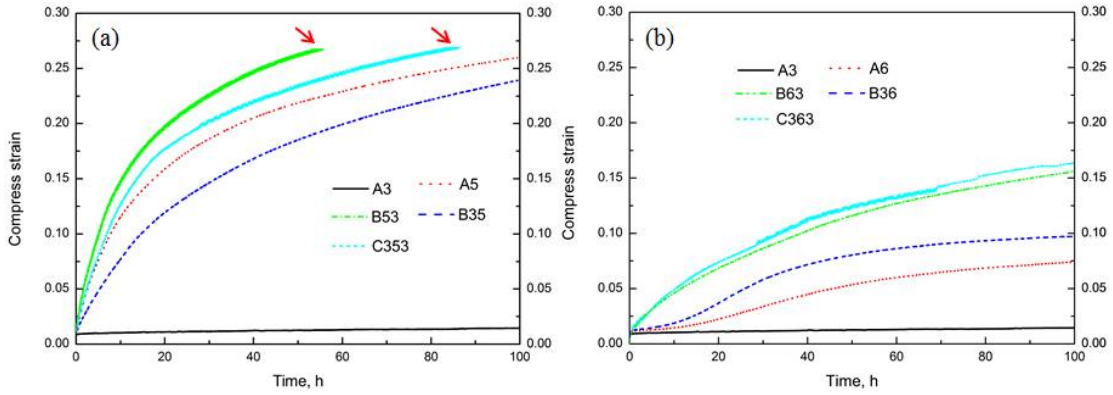

Fig. 7 Creep curves after various heat treatments involved at 500°C (a) and 625°C (b)

According to the compression creep condition applied in present work, the creep mechanism is primarily controlled by the glide and climb of dislocations during creep [34]. However, the difference between various heat treatments is hard to distinguish. Besides, threshold stress σ_{th} and true stress exponent n are reported to be two significant parameters to characterize the creep resistance. Therefore, A3, A5 and A6 have been performed the step-load creep test. The threshold stress σ_{th} is calculated as the stress level when minimum strain rate (ε) is extrapolated to 10^{-10} s^{-1} and true stress exponent is the slope of $\ln\varepsilon$-$\ln(\sigma-\sigma_{th})$ curve [35] and the results are shown in Fig. 8.

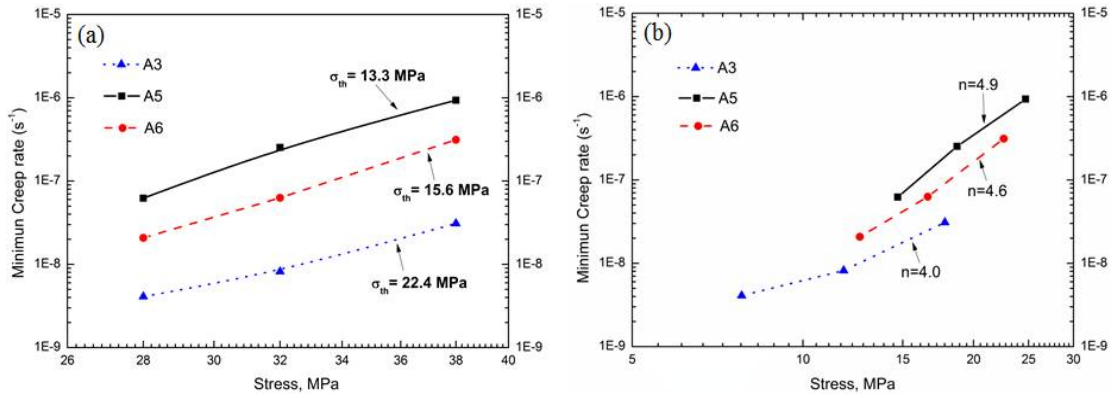

Fig. 8 Threshold stress σ_{th} (a) and stress exponent n (b) in A3, A5 and A6

As shown in Fig. 8a, σ_{th} increases in the order of A5 (13.3 MPa) to A6 (15.6 MPa) and further to A3 (22.4 MPa), indicating the important role of dispersoid (A3) and soluted atoms (A6) in the creep resistance. Though the difference between threshold stress after various heat treatment is not so big, however, an increase of ~ 3MPa in threshold stress can be translated into an order of magnitude decrease in minimum creep according to the literature [36]. In present work, the difference of threshold stress between A6 (15.6 MPa) and A5 (13.3 MPa) is 2.3 MPa but 7 times lower in minimum creep rate in A6 than A5 has been observed in Fig. 8a. Besides, the true stress exponent n

is calculated to be in the range of 4-5 (Fig. 9b), which indicates that the creep is controlled by the dislocation glide or/and climb at elevated temperature [37, 38], confirming the dislocation-control creep mechanism in present work.

Since the creep is confirmed to be controlled by the dislocation glide or/and climb, the factors which can affect the movement of dislocation will have the influence on creep behavior, such as the grain boundary, intermetallics, dispersoids and soluted atoms in present work. From the EBSD measurements, the grain size is found to be similar after all the heat treatments, which is in the range of 340-360 μm. Besides, the intermetallics also show a similar volume fraction (3.8- 4.2 vol. % measured with image analysis). Therefore, the difference in creep resistance, such as σ_{th}, is mainly controlled by the characters of dispersoid and solute level of atoms.

According to the literature, the contribution of dispersoids to σ_{th} can be estimated by the Orowan stress model in the following equation [27]:

$$\sigma_{dispersoid} = \frac{Gb}{4r}\left(\sqrt{\frac{\pi}{4f}} - 1\right)^{-1} \quad (4)$$

On the other hand, the influence of soluted atoms σ_{th} can be expressed in the equation [39]:

$$\sigma_{solute\ atom} = KGCexp(\frac{Q}{RT}) \quad (5)$$

Where, K is a constant. G, b, γ and C have the same meaning with Eqs. (1) - (3) while R is the gas content and T is the absolute temperature. Q is the interaction energy between soluted atom and dislocation, which can be calculated as following [40]:

$$Q = 2G\frac{1+\nu}{1-\nu}(\gamma_1 - \gamma_0)\gamma_0^2 \quad (6)$$

Similar to the evolution of YS, the difference of σ_{th} between A3, A5 and A6 has been calculated: 6.6 MPa between A3 and A6 while 2.3 MPa between A3 and A5, which is close to the experimental data (6.8 MPa between A3 and A6 and 2.3 MPa between A3 and A5), indicating the applicability of model to predict the creep behavior of 3004 alloy in present work. Therefore, the creep threshold stress σ_{th} in other heat treatments has also been calculated using this model and shown in Table 4.

Table 4 Calculated creep threshold stress (σ_{th}) during heat treatments

Code	B35	B53	C353	B36	B63	C363
σ_{th} (MPa)	13.4	12.8	13.1	15.3	14.2	14.5

As shown in Table 4, it can be found that σ_{th} varies with heat treatments though with minor differences and the tendency of evolution is similar with the creep curves shown in Fig. 7. For instance, the total creep strain increases from B35 to C353 and further to B53 (Fig. 7a) while the creep threshold stress also increases in the same order: B35 (13.4 MPa) to C535 (13.1 MPa) and then to B53 (12.8 MPa). In addition, it can be found that the temperature of first-step treatment plays significant role in the evolution of threshold stress. Similar to the evolution of YS, the creep threshold stress with lower temperature in

first-step heat treatments is higher than with higher temperature, which is indicated by the higher creep threshold stress in B35 and B36 than B53 and B63, respectively.

4. Conclusions

(1) Coarsening of dispersoids takes place with increasing temperature from 375°C to 500°C while the dissolution of dispersoids happens with further increased temperature to 625°C. The behaviors including size and distribution of dispersoids as well as the PFZ during various heat treatments have been fully characterized.

(2) The evolution of elevated-temperature strength and creep resistance is greatly related to the temperature of each step during the multi-step heat treatments. The temperature of the first-step heat treatment plays a significant role, in which higher alloy properties can be obtained with lower-temperature heat treatment as the first step while they decrease with increasing temperature of last-step heat.

(3) The creep behavior under all the studied heat treatments is defined as dislocation-controlled mechanism with the stress exponent between 4 and 5 but the creep threshold stress is varying with the heat treatment, which is calculated to be 13-23 MPa.

(4) Suitable models have been preliminarily established to relate the evolution of strength and creep resistance to the behavior of dispersoids and solid-solution level of elements during the studied multi-step heat treatments.

Acknowledgments

The authors would like to acknowledge the financial support of the Natural Sciences and Engineering Research Council of Canada (NSERC) and Rio Tinto Aluminum through the NSERC Industry Research Chair in the Metallurgy of Aluminum Transformation at University of Quebec at Chicoutimi and The Doctoral Start-up Fund of Liaoning Province (No. 20170520403) in Northeastern University.

Author Contributions: G. S. Wang, K. Liu and S. L. Wang conceived and designed the experiments; G. S. Wang and K. Liu performed the experiments; K. Liu analyzed the data; G. S. Wang wrote the paper and K. Liu modified the paper.

Conflicts of Interest: The authors declare no conflict of interest.

References

[1] J.G. Kaufman, Properties of aluminum alloys : tensile, creep, and fatigue data at high and low temperatures, ASM International ; Aluminum Association, Materials Park, Ohio; Washington, D.C., 1999.

[2] I.J. Polmear, M.J. Couper. Design and development of an experimental wrought aluminum alloy for use at elevated temperatures. *Metall. Trans. A,* **1988,** *19,* 1027-1035. 10.1007/BF02628387.
[3] M.E. Van Dalen, T. Gyger, D.C. Dunand, D.N. Seidman. Effects of Yb and Zr microalloying additions on the microstructure and mechanical properties of dilute Al–Sc alloys. *Acta Mater.,* **2011,** *59,* 7615-7626. 10.1016/j.actamat.2011.09.019.
[4] J. Lai, Z. Zhang, X.G. Chen. The thermal stability of mechanical properties of Al–B4C composites alloyed with Sc and Zr at elevated temperatures. *Mater. Sci. Eng., A,* **2012,** *532,* 462-470. 10.1016/j.msea.2011.11.013.
[5] A.R. Farkoosh, X. Grant Chen, M. Pekguleryuz. Dispersoid strengthening of a high temperature Al–Si–Cu–Mg alloy via Mo addition. *Mater. Sci. Eng., A,* **2015,** *620,* 181-189. http://dx.doi.org/10.1016/j.msea.2014.10.004.
[6] K. Liu, H. Ma, X.G. Chen. Enhanced elevated-temperature properties via Mo addition in Al-Mn-Mg 3004 alloy. *J. Alloys Compd. ,* **2017,** *694,* 354-365. http://dx.doi.org/10.1016/j.jallcom.2016.10.005.
[7] Y.J. Li, A.M.F. Muggerud, A. Olsen, T. Furu. Precipitation of partially coherent α-Al(Mn,Fe)Si dispersoids and their strengthening effect in AA 3003 alloy. *Acta Mater.,* **2012,** *60,* 1004-1014. 10.1016/j.actamat.2011.11.003.
[8] K. Liu, X.-G. Chen. Evolution of microstructure and elevated-temperature properties with Mn addition in Al-Mn-Mg alloys. *J. Mater. Res. ,* **2017,** *32,* 2585-2593. doi:10.1557/jmr.2017.239.
[9] K. Liu, X.G. Chen. Development of Al–Mn–Mg 3004 alloy for applications at elevated temperature via dispersoid strengthening. *Mater. Des.,* **2015,** *84,* 340-350. http://dx.doi.org/10.1016/j.matdes.2015.06.140.
[10] K. Liu, X.G. Chen. Evolution of Intermetallics, Dispersoids, and Elevated Temperature Properties at Various Fe Contents in Al-Mn-Mg 3004 Alloys. *Metall. Mater. Trans. B,* **2015,** *47B,* 3291-3300. 10.1007/s11663-015-0564-y.
[11] K. Liu, X.G. Chen. Influence of heat treatment and its sequence on elevated-temperature properties of Al-Mn-Mg 3004 alloy. *Mater. Sci. Eng. A,* **2017,** *697,* 141-148. https://doi.org/10.1016/j.msea.2017.05.027.
[12] K. Liu, A.M. Nabawy, X.-G. Chen. Influence of TiB2 nanoparticles on the elevated-temperature properties of Al-Mn-Mg 3004 alloy. *Trans. Nonferrous Met. Soc. China,* **2017,** *27,* 771-778. DOI: 10.1016/S1003-6326(17)60088-8.
[13] J. Cadek. Creep in precipitation- and dispersion-strengthened alloys (a review). *Kovove Mater. ,* **1991,** *29,* 385-398.
[14] K.E. Knipling, D.C. Dunand, D.N. Seidman. Criteria for developing castable, creep-resistant aluminum-based alloys - A review. *Z. METALLKD,* **2006,** *97,* 246-265. 10.3139/146.101249
[15] A.W. Zhu, B.M. Gable, G.J. Shiflet, E.A. Starke Jr, in: P.J. Gregson, S. Harris (Eds.) Aluminium Alloys 2002 Their Physical and Mechnaical Properties: Proceedings of the 8th International Conference ICAA8, Cambridge, 2002, pp. 21-30.
[16] K.E. Knipling, D.C. Dunand. Creep resistance of cast and aged Al–0.1Zr and Al–0.1Zr–0.1Ti (at.%) alloys at 300–400 °C. *Scr. Mater.,* **2008,** *59,* 387-390. http://dx.doi.org/10.1016/j.scriptamat.2008.02.059.

[17] M.E. Krug, D.C. Dunand. Modeling the creep threshold stress due to climb of a dislocation in the stress field of a misfitting precipitate. *Acta Mater.,* **2011,** *59,* 5125-5134. http://dx.doi.org/10.1016/j.actamat.2011.04.044.

[18] E.A. Marquis, D.C. Dunand. Model for creep threshold stress in precipitation-strengthened alloys with coherent particles. *Scr. Mater.,* **2002,** *47,* 503-508. http://dx.doi.org/10.1016/S1359-6462(02)00165-3.

[19] D.N. Seidman, E.A. Marquis, D.C. Dunand. Precipitation strengthening at ambient and elevated temperatures of heat-treatable Al(Sc) alloys. *Acta Mater.,* **2002,** *50,* 4021-4035. 10.1016/S1359-6454(02)00201-X.

[20] P.X. Liu, Y. Liu, R. Xu. Microstructure quantitative analysis of directionally solidified Al-Ni-Y ternary eutectic alloy. *Trans. Nonferrous Met. Soc. China,* **2014,** *24,* 2443-2451.

[21] E.R. Weibel, H. Elias, Quantitative methods in morphology, Springer-Verlag, Berlin; New York, 1967.

[22] Y.J. Li, L. Arnberg. Quantitative study on the precipitation behavior of dispersoids in DC-cast AA3003 alloy during heating and homogenization. *Acta Mater.,* **2003,** *51,* 3415-3428. http://dx.doi.org/10.1016/S1359-6454(03)00160-5.

[23] Y. Li, L. Arnberg, Precipitation of Dispersoids in DC-Cast AA31O3 Alloy during Heat Treatment, Essential Readings in Light Metals,in: F. Grandfield, D.G. Eskin (Ed.)^(Eds.) John Wiley & Sons, Inc., Hoboken, NJ, USA, 2013, pp. 1021-1027.

[24] H.-W. Huang, B.-L. Ou. Evolution of precipitation during different homogenization treatments in a 3003 aluminum alloy. *Mater. Des.,* **2009,** *30,* 2685-2692. 10.1016/j.matdes.2008.10.012.

[25] Y.J. Li, L. Arnberg. Evolution of eutectic intermetallic particles in DC-cast AA3003 alloy during heating and homogenization. *Mater. Sci. Eng., A,* **2003,** *347,* 130-135. 10.1016/s0921-5093(02)00555-5.

[26] A.M.F. Muggerud, E.A. Mørtsell, Y. Li, R. Holmestad. Dispersoid strengthening in AA3xxx alloys with varying Mn and Si content during annealing at low temperatures. *Mater. Sci. Eng., A,* **2013,** *567,* 21-28. 10.1016/j.msea.2013.01.004.

[27] R.A. Karnesky, L. Meng, D.C. Dunand. Strengthening mechanisms in aluminum containing coherent Al3Sc precipitates and incoherent Al2O3 dispersoids. *Acta Mater.,* **2007,** *55,* 1299-1308. http://dx.doi.org/10.1016/j.actamat.2006.10.004.

[28] E.L. Huskins, B. Cao, K.T. Ramesh. Strengthening mechanisms in an Al–Mg alloy. *Mater. Sci. Eng., A,* **2010,** *527,* 1292-1298. http://dx.doi.org/10.1016/j.msea.2009.11.056.

[29] S. Kahl, H.-E. Ekström, J. Mendoza. Tensile, Fatigue, and Creep Properties of Aluminum Heat Exchanger Tube Alloys for Temperatures from 293 K to 573 K (20 °C to 300 °C). *Metall. Mater. Trans. A,* **2014,** *45,* 663-681. 10.1007/s11661-013-2003-5.

[30] Q. Zhao, Department of Materials Science and Engineering, Norwegian University of Science and Technology, Trondheim, 2013.

[31] A.V. Kazantzis, Z.G. Chen, J.T.M. De Hosson. Deformation mechanism of aluminum–magnesium alloys at elevated temperatures. *J. Mater. Sci.,* **2013,** *48,* 7399-7408. 10.1007/s10853-013-7555-7.

[32] C. Shi, X.G. Chen. Effect of vanadium on hot deformation and microstructural evolution of 7150 aluminum alloy. *Mater. Sci. Eng., A,* **2014,** *613,* 91-102. http://dx.doi.org/10.1016/j.msea.2014.06.082.

[33] O.D. Sherby, A. Goldberg, O.A. Ruano. Solute-diffusion-controlled dislocation creep in pure aluminium containing 0.026 at.% Fe. *Philos. Mag.,* **2004,** *84,* 2417-2434. 10.1080/14786430410001690006.

[34] G.E. Dieter, Mechanical metallurgy, McGraw-Hill, New York, 1986.

[35] S.P. Deshmukh, R.S. Mishra, K.L. Kendig. Creep behavior and threshold stress of an extruded Al–6Mg–2Sc–1Zr alloy. *Mater. Sci. Eng., A,* **2004,** *381,* 381-385. http://dx.doi.org/10.1016/j.msea.2004.05.025.

[36] A.R. Farkoosh, X.G. Chen, M. Pekguleryuz. Interaction between molybdenum and manganese to form effective dispersoids in an Al–Si–Cu–Mg alloy and their influence on creep resistance. *Mater. Sci. Eng., A,* **2015,** *627,* 127-138. http://dx.doi.org/10.1016/j.msea.2014.12.115.

[37] Y. Li, S.R. Nutt, F.A. Mohamed. An investigation of creep and substructure formation in 2124 Al. *Acta Mater.,* **1997,** *45,* 2607-2620. http://dx.doi.org/10.1016/S1359-6454(96)00367-9.

[38] F.A. Mohamed, K.-T. Park, E.J. Lavernia. Creep behavior of discontinuous SiC Al composites. *Mater. Sci. Eng., A,* **1992,** *150,* 21-35. http://dx.doi.org/10.1016/0921-5093(90)90004-M.

[39] Z. Lin, Y. Li, F.A. Mohamed. Creep and substructure in 5 vol.% SiC-2124Al composite. *Mater. Sci. Eng., A,* **2002,** *332,* 330-342. http://dx.doi.org/10.1016/S0921-5093(01)01760-9.

[40] H. Watanabe, T. Mukai, K. Higashi. Influence of Temperature and Grain Size on Threshold Stress for Superplastic Flow in a Fine-Grained Magnesium Alloy. *Metall. Mater. Trans. A,* **2008,** *39,* 2351-2362. 10.1007/s11661-008-9596-0.